UM-P-82/53

A COLLECTIVE MODEL DESCRIPTION OF THE LOW LYING AND GIANT DIPOLE RESONANT PROPERTIES OF $^{40,42,44,46}Ca$.

J. I. WEISE.

C/O

SCHOOL OF PHYSICS,

UNIVERSITY OF MELBOURNE,

PARKVILLE, VICTORIA. 3052.

AUSTRALIA.

ABSTRACT: The low lying and giant dipole resonant properties of the even-even calcium isotopes are calculated within the framework of the Gneuss-Greiner model and compared with the experimental data. In the low energy region, comparison is also made with the predictions of a coexistence model.

1. INTRODUCTION

Although ^{40}Ca has a doubly closed shell at N and Z equals 20, the closure is far from perfect. Evidence for this includes transition rates enhanced over single particle estimates, rotational band structure and the presence of low lying 0^+-states unexplained in terms of simple pf shell model configurations. This led Gerace and Green [1], Federman and Pittel [2] and others [3,4,5] to propose that the wave functions of the low lying states of the even-even calcium isotopes ($^{40,42,44,46}Ca$) are admixtures of spherical and multiparticle-multihole deformed basis states, that is, (^{40}Ca-) core-excited states. With the introduction of such complicated configurations, better agreement with these low lying features has been obtained, but at considerable computational expense. An alternative model therefore, providing a simpler account of the particular low lying features of interest, would be desirable.

The need to include core-excited nucleons indicates the importance of collective correlations in these nuclei and thus provides the basis for a collective model approach. Of the collective (and single particle) models available, the Gneuss-Greiner model [6] as extended by Rezwani et al. [7] provides, in addition, a description of features in the giant dipole resonant region. With the advent of recent photonuclear cross section experiments at Tohoku University and here at Melbourne using enriched ^{42}Ca and ^{44}Ca targets, a description in this region is of considerable interest.

The model of Gneuss and Greiner as applied to the low energy and giant dipole resonant properties of even-even nuclei is presented in section 2. For the low lying features, only properties arising from quadrupole modes of surface vibrations can be adequately described within this model. Further, how well the Gneuss-Greiner

model can reproduce these low lying features within these degrees of freedom will affect the reliability of the description in the giant dipole resonant (GDR) region. Fortunately however, this relies largely only on a few of the low lying states. Furthermore as shown in section 3, where the results of the calculation are presented and discussed, the predicted low lying features compare favourably with those of a coexistence model and the experimental data. The coexistence model is based on admixtures of shell model and deformed components coexisting in the low lying states, and possibly represents the simplest of the 'shell model' approaches. Even so, this approach is far more complicated than that of the Gneuss-Greiner model which has the added bonus of being easily extended into the GDR region. Except for ^{40}Ca [8], few shell model calculations for nuclei with $A>40$ have been attempted in this region.

2. THEORY

The total Hamiltonian coupling the giant dipole resonant states to the low energy states is given by

$$H = H_Q + H_D + H_{DQ} \tag{1}$$

where H_Q describes the low energy quadrupole degrees of freedom in terms of the collective coordinate α and their conjugate momenta π,

$$H_Q = P_2[\pi^{[2]} \times \pi^{[2]}]^{[0]} + P_3[\pi^{[2]} \times \alpha^{[2]} \times \pi^{[2]}]^{[0]} + C_2L_2 + C_3L_3 + C_4L_2^2 + C_5L_2L_3 + C_6L_3^2 + D_6L_2^3 ; \tag{2}$$

$$L_2 = [\alpha^{[2]} \times \alpha^{[2]}]^{[0]} , \quad L_3 = [\alpha^{[2]} \times \alpha^{[2]} \times \alpha^{[2]}]^{[0]}.$$

Once the mass parameters (P_2 and P_3) of the kinetic energy term and the inertia parameters (C_2, C_3, C_4, C_5, C_6 and D_6) of the potential energy term have been defined, this Hamiltonian, H_Q can be diagonalised for each of the angular momenta 0, 2, 3, 4, 5 and 6 using linear combinations of the eigenstates of the five-dimensional harmonic oscillator as the basis, viz.

$$|\gamma, Lm\rangle = \sum_{N\nu\alpha} C^{\gamma}(N\nu L\alpha) \; |[N]\nu L\alpha m\rangle, \tag{3}$$

thus yielding energy levels and eigenstates. These eigenstates are then used to calculate the quadrupole moment of a state $|\gamma, Lm\rangle$ and the reduced E2 transition probability between an initial state $|\gamma, Lm\rangle$ and a final state $|\gamma', L'm'\rangle$ according to :

$$Q(\gamma, Lm{=}L) = \sqrt{\frac{16\pi}{5}} \begin{pmatrix} L & 2 & L \\ -L & 0 & L \end{pmatrix} \langle \gamma, L \| Q^{[2]} \| \gamma, L\rangle \tag{4a}$$

and $$B(E2{:}\gamma, L \to \gamma', L') = (2L+1)^{-1} \left| \langle \gamma', L' \| Q^{[2]} \| \gamma, L\rangle \right|^2. \tag{4b}$$

The quadrupole operator is defined by a homogeneous charge distribution ρ_0, whence to second order in α

$$Q_{2\mu} = \int \rho(r)\, r^2\, Y_{2\mu}\, d\tau = \rho_0 R_0^5 \, (\alpha_{2\mu} - 10(70\pi)^{-1/2} \, [\alpha^{[2]} \times \alpha^{[2]}]^{[2]}_{\mu}). \tag{5}$$

H_D in (1) is the Hamiltonian of the giant dipole resonance,

which can be defined in terms of creation and annihilation operators, $q_\nu^{[1]\dagger}$ and $q_\nu^{[1]}$, for dipole phonons of unperturbed energy $\hbar\omega_1$, as:

$$H_D = \sqrt{3}\,\hbar\omega_1\,[q^{[1]\dagger} \times q^{[1]}]^{[0]}. \tag{6}$$

H_{DQ} is the interaction term from the coupling of the dipole and quadrupole degrees of freedom,

$$H_{DQ} = \hbar\omega_1 B_1\,[q^{[1]\dagger} \times q^{[1]} \times \alpha^{[2]}]^{[0]} + \hbar\omega_1 \sum_{j=0,2} B_{2j}[q^{[1]\dagger} \times q^{[1]} \times [\alpha^{[2]} \times \alpha^{[2]}]^{[j]}]^{[0]}, \tag{7}$$

where the coupling constants B_1, B_{20} and B_{22} are determined uniquely from a hydrodynamical model.

The eigenstates of the total Hamiltonian H can be expanded in terms of product states of the five-dimensional quadrupole and three-dimensional dipole oscillators, namely

$$H\,|n,I=1,M\rangle = E_n\,|n,I=1,M\rangle \tag{8a}$$

$$|n,I=1,M\rangle = \sum_{N\nu\alpha L} C^n(N\nu\alpha L)\,(Lm1m'|1M)\,|[N]\nu L\alpha m\rangle_Q \cdot |[1]1m'\rangle_D \tag{8b}$$

where $|[1]1m'\rangle_D = q^\dagger_{m'}\,|0\rangle$.

From the dipole operator,

$$D^{[1]} = M_0(q^{[1]\dagger} + q^{[1]} + M_1[(q^{[1]\dagger} + q^{[1]}) \times \alpha^{[2]}]^{[1]} + \sum_{j=0,2} M_{2j}[(q^{[1]\dagger} + q^{[1]}) \times (\alpha^{[2]} \times \alpha^{[2]})^{[j]}]^{[1]}), \tag{9}$$

(where $M_0 = 0.654\hbar\sqrt{(NZ(1+\alpha)/AM\hbar\omega_1)}$, $M_1 = -0.554$, $M_{20} = 0.011$, $M_{22} = 0.100$, and α is the effective-mass parameter), the two following features in the GDR region are calculated:

(i) The total γ-ray absorption cross section

$$\sigma(E) = \frac{8\pi e^2}{3\hbar c} \sum \left|\langle n,I=1 \| D \| 0\rangle\right|^2 \frac{E_n\Gamma_n}{(E^2-E_n^2)^2/E^2+\Gamma_n^2}, \tag{10}$$

where E_n and Γ_n are the energies and widths respectively of the GDR states $|n,I=1,M\rangle$, and $|0\rangle$ represents the ground state of H_D and H_Q.

(ii) The γ-ray scattering cross section

$$\frac{d\sigma_{0\to I_f}(E,\theta)}{d\Omega} = \frac{E'}{E}\left|P_{I_f}\right|^2 g_{I_f}(\theta), \tag{11}$$

where the angular distributions are

$$g_0 = (1+\cos^2\theta)/6, \quad g_1 = (2+\sin^2\theta)/4, \quad g_2 = (13+\cos^2\theta)/12,$$

θ is the scattering angle, and E and E' are the energies of the incident and scattered photons respectively. The polarizabilities are

$$P_{I_f} = \frac{1}{\sqrt{3}(2I_f+1)} \frac{EE'}{(\hbar c)^2} \sum_n \langle I_f \| D^{[1]} \| 1_n \rangle \langle 1_n \| D^{[1]} \| 0 \rangle$$

$$\times \frac{1}{E_n+E'+i\Gamma_n/2} + \frac{(-)^j}{E_n-E-i\Gamma_n/2} - \frac{\delta_{I_f 0}\sqrt{3}(Ze)^2}{AMc^2}.$$

where $|1_n\rangle \equiv |n, I=1\rangle$

Finally, a physical insight into the nuclear structure of a nucleus can be gained via the collective potential energy surface. This is obtained by expressing the potential energy part of H_0 in terms of the deformation parameters β and γ or a_0 and a_2, viz.

$$\begin{aligned} V(a_0,a_2) &= C_2(a_0^2 + 2a_2^2)/\sqrt{5} + C_3\sqrt{(2/35)}\, a_0(6a_2^2 - a_0^2) \\ &+ C_4(a_0^2 + 2a_2^2)^2/5 + C_5\sqrt{(2/175)}\,(a_0^2 + 2a_2^2)a_0(6a_2^2 - a_0^2) \\ &+ C_6 2a_0^2(6a_2^2 - a_0^2)^2/35 + D_6(a_0^2 + 2a_2^2)^3/\sqrt{125}\,, \end{aligned} \tag{12}$$

where $a_0 = \beta\cos\gamma$ and $a_2 = (\beta\sin\gamma)/\sqrt{2}$. The most important feature in a potential energy surface (PES) is the deepest minimum which generally determines the deformation of the ground state with its depth being a measure of the stability of this particular shape.

3. RESULTS AND DISCUSSION.

The final low energy parameters of H_Q are obtained from the initial parameters of Sedlmayr [9] by reduced χ^2 fitting, as faithfully as possible, a number of low energy features (such as the energies of the 0_2^+, 2_1^+, 2_2^+ and 4_1^+ states, B(E2) values for the transitions $4_1^+ \rightarrow 2_1^+$, $0_2^+ \rightarrow 2_1^+$ and $2_1^+ \rightarrow 0_1^+$ and the quadrupole moment of the 2_1^+-state) which are both reliably known and crucial in defining the category to which the nucleus belongs or lies between, in the limiting collective models of either spherical vibrational or permanently deformed. The resultant parameters obtained for the calcium isotopes are presented in Table 1.

3.1 LOW LYING FEATURES.

Qualitatively from the PES presented in Fig. 1, the ground state of ^{40}Ca belongs to the spherical minimum and the positive parity states to the asymmetric minimum. This compares favourably with what is found experimentally. The ground state of ^{40}Ca is essentially spherical [10] whilst the lowest lying positive parity states are members of the two rotational bands, $K = 0^+$ (β-band) and $K = 2^+$ (γ-band), built upon 4p-4h deformed states [11] (with higher energy states forming $K = 0^+$ 2p-2h and 8p-8h bands [12]). These energy levels have been presented in Fig. 2 and compared with the Gneuss-Greiner model calculation. The change in sign of the calculated quadrupole moments from negative for the 2_1^+-state to positive for the 2_2^+-state supports the K-band assignment of these states. Further in Table 2 where the B(E2) transition rates as predicted by the Gneuss-Greiner and the coexistence models are compared with the data, the Gneuss-Greiner model reproduces the properties of both experimental 4p-4h rotational bands satisfactorily. Indeed the Gneuss-Greiner model description is as good as that of the

coexistence model. The features of the low lying levels of ^{40}Ca being highly collective in nature provide a firm basis for the Gneuss-Greiner model calculation. Therefore, it will be of interest how well this calculation reproduces the structure in the GDR region.

The quadrupole moment of ^{40}Ca has not been measured. However, based on the similarities in the properties of the low lying deformed states of ^{42}Ca and ^{40}Ca and the measured prolate deformation of the lowest rotational band in ^{42}Ca, Cline and coworkers proposed that the lowest $K = 0^+$ rotational band in ^{40}Ca should have a prolate deformation [13]. This is consistent with the sign of the quadrupole moment of the 2_1^+-state of ^{40}Ca as calculated by the Gneuss-Greiner model as well as with both the α-transfer data to 4p-4h states in ^{40}Ca [11] and studies made by Gerace and Green [1]. However it is not in agreement with reports by Braun-Munzinger et al. [14] of an oblate deformation.

As depicted in the PES of Fig. 1, the ground states of ^{42}Ca and ^{44}Ca belong to the 'spherical' and soft prolate minima respectively. The positions of the 2_1^+, 4_1^+ and 6_1^+ levels of $^{42,44,46}Ca$ have been satisfactorily accounted for with conventional shell model calculations using effective two-body interactions assuming an inert ^{40}Ca core and predominantly $1f_{7/2}$ and $2p_{3/2}$ neutrons [4,15]. However enhanced E2 transition rates (noteably the $2_1^+ \rightarrow 0_1^+$ transition) have warranted the inclusion of deformed components (specifically 4p-2h in ^{42}Ca [16,17] and 6p-2h in ^{44}Ca [18]) in the wave functions of these members of the ground state band in $^{42,44}Ca$. Similarly the 0_2^+ and 2_2^+ levels missing in this description have been interpreted as core excited levels in analogy with the excited states (specifically the 0_2^+ and 2_1^+ levels) of ^{40}Ca [4,5]; these deformed states arise mainly from a two-proton excitation from the sd- to pf-shell [19,20]. This core

deformation decreases as neutrons are added to the ^{40}Ca core [21] as exemplified in the PES of ^{46}Ca which clearly resembles that of an anharmonic vibrator. Indeed in ^{48}Ca, core excitation plays no significant role [5].

As shown in Fig. 3, the calculated energy levels and quadrupole moments of ^{42}Ca and ^{44}Ca adequately reproduce the experimental data. However in Table 3, where the calculated reduced E2 transition rates of ^{42}Ca are compared with the predictions of the coexistence model [16] and the data, the transition rates (denoted with an asterisk) involving the higher angular momentum states and the 2_3^+ state have been grossly overestimated in the Gneuss-Greiner model calculation. It appears that the collectivity, which was introduced in order to fit the quadrupole moment and low lying ($2_1^+ \rightarrow 0_1^+$, $2_1^+ \rightarrow 0_2^+$) enhanced transition rates, has increased with excitation energy such that the 6_1^+ state, for example, has been predicted as highly collective in contrast to what is found experimentally and by the coexistence model calculation where the composition of the 6_1^+-state is 92% $\nu(f_{7/2})^2$ [16]. It should be noted that no improvement could be made on the initial PES of ^{42}Ca as calculated by Sedlmayr. Perhaps therefore another starting PES may provide a better description of this nucleus.

In Table 4, the compositions of the levels in the coexistence model of ^{42}Ca [19] are compared with those of ^{40}Ca [22]. The states in ^{40}Ca are purer (essentially multiparticle-multihole deformed) than ^{42}Ca where more configuration mixing of shell model states occurs. The presence of these single particle aspects pose considerable problems for the Gneuss-Greiner model.

A similar situation arises for ^{44}Ca as shown in Table 5 where the calculated E2 transition rates of ^{44}Ca are compared with the

coexistence model predictions and with experiment. The majority of the transition rates are reproduced by the Gneuss-Greiner model except those involving the 6_1^+-state (denoted with an asterisk) which are overestimated. As shown in Table 6, where the composition of the levels of ^{44}Ca according to McCullen and Donahue [18] are presented, the amount of deformed wave function admixtures in the states, introduced mainly to reproduce the transition rates forbidden seniority-wise, is substantial.

The PES of ^{46}Ca, and hence the low lying properties as presented in Fig. 4, is typical of an anharmonic vibrator. Unfortunately little experimental data exists with which to compare these calculations.

3.2 GIANT DIPOLE RESONANT REGION.

In the previous section it was found that the Gneuss-Greiner model failed to describe the low energy properties of the higher angular momentum states. Nonetheless this should not significantly affect the predictions of the model in the GDR region since only those states with angular momenta 0 and 2 enter into the interaction. Further, of these states, the 0_1^+ and 2_1^+ states will have the greatest influence and the features of these compare favourably with the data; indeed the majority of the low energy properties of these states were χ^2-fitted. Since the surface properties of the ground state largely determine the energy and shape of the GDR, the predictions will mainly reflect shape transitions across the isotopes.

The main decay modes of the total E1 absorption cross section are in the (γ,n) and (γ,p) channels, which, in this atomic mass region, have approximately equal weight. Therefore in the following comparisons, these two partial cross sections are summed to approximate the total experimental γ-ray absorption cross section.

In the calculations presented, the energy $\hbar\omega_1$ of the unperturbed dipole state and the widths Γ_n of the dipole strengths were taken as 20.5MeV and 3.0MeV respectively to be consistent with the data. Since uncertainties in $\hbar\omega_1$ and the effective nucleon mas (taken as M) may affect the overall cross section strengths, not too much emphasis should be placed on the agreement between the energy positions and cross section magnitudes but rather how well the relative positions and strengths of the dipole states correspond to the data.

The nucleus ^{40}Ca has a PES with two minima, one for a spherical shape and the other for an asymmetric deformed shape. Since the two minima are well separated, the ground state of ^{40}Ca, belonging to the spherical minimum, is largely independent of the excited states which occur at quite high excitation energies (>3MeV) and belong to the deformed minimum. Consequently, the γ-ray absorption cross section should resemble that of a spherical nucleus, that is, essentially a single major dipole strength with the only inelastic γ-ray scattering expected to occur into the 2^+ vibrational one-phonon state. However none of the 2^+-states investigated here exhibit this character and hence no appreciable inelastic γ-ray scattering occurs into any of the excited states of ^{40}Ca (see Fig. 9). In Fig. 5 the Gneuss-Greiner model prediction (full curve) of the photoabsorption cross section of ^{40}Ca is compared with the photoproton and photoneutron cross section data. With the unperturbed dipole energy $\hbar\omega_1$ taken as 20.0MeV, the predictions comfortably overlap the data.

The γ-ray absorption cross sections of ^{42}Ca and ^{44}Ca, according to the Gneuss-Greiner model, should reflect the structure of nuclei with shapes between spherical and prolate deformed. Although the ground state of ^{42}Ca is predominantly spherical, some mixing will

occur with the shallow prolate minimum, so that in addition to the main vibrational strengths, there will be considerable strength elsewhere across the GDR region (as shown in Fig. 6) due to this rotation-vibration interaction Since the prolate minimum of ^{44}Ca is deeper than that of ^{42}Ca, there will be increased strength in the γ-ray absorption (and the elastic scattering) cross section of ^{44}Ca where the two transverse dipole modes associated with this prolate minimum occur (~22MeV in Fig. 7). Although the predicted cross section is underestimated for ^{42}Ca, the correspondence between the predicted structure and that observed for $^{42,44}Ca$ is striking.

The predicted γ-ray absorption cross section of ^{46}Ca as presented in Fig. 8 resembles that of an anharmonic vibrator. As yet, there are no measured photoabsorption cross section data for ^{46}Ca available with which to compare this prediction. As for ^{40}Ca, the only significant inelastic γ-ray scattering predicted for $^{42,44,46}Ca$ is into the one-phonon vibrational 2^+-state belonging to the ground state 'spherical' minimum (see Fig. 9). Unfortunately there are no inelastic γ-ray scattering data available for the calcium isotopes with which to compare these predictions.

4. CONCLUSIONS.

The Gneuss-Greiner model predicts many of the low energy and giant dipole resonant features of the even-even calcium isotopes. Further data in the GDR region and, in particular, γ-ray scattering cross section measurements would provide a more informative means of testing model predictions and ultimately of probing the nuclear structure of these nuclei.

Some such measurements in the medium to heavy atomic mass region have been reported by Arenhovel and Maison [26] and more recently by Bowles et al. [27] and Nathan and Morch [28]. All compare their data with a dynamic collective model (DCM) calculation. There is some evidence that the DCM tends to overestimate the inelastic γ-ray scattering data by a factor of 2 to 3. For ^{48}Ti and ^{52}Cr, the data of Arenhovel and Maison has been discussed within the present calculation, and indeed some discrepancy in the magnitudes has occured [29].

Further, in some cases, the DCM could not reliably reproduce the structure present in these photon scattering data. Bowles et al. by incorporating isospin splitting, in an ad hoc manner, into the DCM have improved the fits somewhat.

Still the Gneuss-Greiner model certainly provides a relatively easy and quite successful calculation of the collective properties of a range of nuclei. The main failure is, as expected, its inadequacy in dealing with single particle degrees of freedom. Since the measured inelastic γ-ray scattering data are much less than predicted by this collective model, a microscopic description may be more applicable

REFERENCES:

1. Gerace, W.J., Green, A.M.: Nucl. Phys. A93, 110 (1967)
   Gerace, W.J., Green, A.M.: Nucl. Phys. A113, 641 (1968)
   Gerace, W.J., Green, A.M.: Nucl. Phys. A123, 241 (1969)
2. Federman, P., Pittel, S.: Phys. Rev. 186, 1106 (1969)
   Federman, P., Pittel, S.: Nucl. Phys. A139, 108 (1969)
   Federman, P., Pittel, S.: Nucl. Phys. A155, 161 (1970)
3. Lippincott, E.P., Bernstein, A.M.: Phys. Rev. 163, 1170 (1967)
   McGrory, J.B., Wildenthal, B.H.: Phys. Lett. 28B, 237 (1968)
   McDonald, J.R. et al.: Phys. Rev. C3, 219 (1971)
4. McGrory, J.B. et al.: Phys. Rev. C2, 186 (1970)
5. Banerjee, D., Oberlechner, G.: Phys. Rev. C7, 2437 (1973)
6. Gneuss, G., Greiner, W.: Nucl. Phys. A171, 449 (1971)
7. Rezwani, V., Gneuss, G., Arenhovel, H.: Nucl. Phys. A180, 254 (1972)
8. Brown, G.E. et al.: Nucl. Phys. 22, 1 (1961)
   Weigert, L.J., Eisenberg, J.M.: Nucl. Phys. 53, 508 (1964)
   Gillet, V., Sanderson, E.A.: Nucl. Phys. 54, 472 (1964)
   Hill, L.L.: Phys. Lett. 25B, 169 (1967)
   Marangoni, M., Saruis, A.M. Nucl. Phys. A132, 649 (1969)
   Wong, S.S.M. et al.: Phys. Lett. 48B, 403 (1974)
9. Sedlmayr, R.: 1976 Dissertation, Universitat Frankfurt am Main.
10. Hubbard, L.B. et al.: Phys. Rev. C6, 532 (1972)
11. Betts, R.R. et al.: Nucl. Phys. A292, 281 (1977)
12. Fortune, H.T. et al.: Phys. Lett. 55B, 439 (1975)
    Sukakura, M. et al.: Phys. Lett. 61B, 335 (1976)
13. Towsley, C.W. et al. Phys. Rev. Lett. 28, 368 (1972)
    Towsley, C.W. et al.: Nucl. Phys. A204, 574 (1973)
    Cline, D. et al.: J.Phys. Soc. Jap. 34, Supplement 344 & 377

14. Braun-Munzinger, P. et al.: Phys. Rev. Lett. 29, 1261 (1972)

15. Wust, N. et al.: J. Phys. G1, 57 (1975)

Kutschera, W. et al.: Phys. Rev. C12, 813 (1975)

Kutschera, W. et al.: Riv. Nuovo Cim. 1, No.12, 3 (1978)

Poletti, A.R. et al.: Phys. Rev. C10, 997 (1974)

16. Flowers, B.H., Skouras, L.D.: Nucl. Phys. A136, 353 (1969)

Lawley, N. et al.: Nucl. Phys. A159, 385 (1970)

17. Kossler, W.J. et al.: Phys. Rev. 177, 1725 (1969)

Ellegaard, G. et al.: Phys. Lett. 40B, 641 (1972)

18. McCullen, J.D. Donahue, D.J.: Phys. Rev. C8,1406 (1973)

19. Flowers. B.H. Skouras, L.D.: Nucl. Phys. A116, 529 (1968)

20. Dupont,Y. et al. Phys. Rev. C7, 637 (1973)

Skouras, L.D.: Nucl. Phys. A220, 604 (1974)

21. Becker, J.A. et al.: Phys. Rev. C10, 99 (1974)

22. Gerace, W.J., Mestre, J.P.: Nucl. Phys. A285, 253 (1977)

23. Baglin, J.E.E., Spicer, B.M : UM-P-63/13 (University of Melbourne)

Brajnik, D. et al.: Phys. Rev. C9, 1901 (1974)

24. Assifiri, Y.I., Thompson, M.N.: Nucl. Phys. A357, 429 (1981)

25. Harty, P.D., Thompson, M.N.: Aust. J. Phys. 34, 505 (1981)

26. Arenhovel, H , Maison, J.M.: Nucl. Phys. A147, 305 (1970)

27. Bowles, T.J. et al.: Phys. Rev. C24, 1940 (1981)

28. Nathan, A.M., Morch, R.: Phys. Lett. B91, 38 (1980)

29. Weise, J.: Zeit. fur. Physik A300, 329 (1981)

Weise, J. Aust. J. Phys. 34, 627 (1981)

TABLE CAPTIONS:

Table 1: Low energy parameters for $^{40,42,44,46}Ca$ used in the present calculation - mass parameters P_2 and P_3 are in units of $10^{40}(MeVsec^2)^{-1}$ and stiffness parameters C_2, C_3, C_4, C_5, C_6, D_6 in units of MeV.

Table 2: Comparison of experimental reduced E2 transition rates in ^{40}Ca and those predicted by the coexistence and Gneuss-Greiner models.

Table 3: Comparison of experimental reduced E2 transition rates in ^{42}Ca with those predicted by the coexistence and Gneuss-Greiner models.

Table 4: Composition of states in $^{40,42}Ca$ as per the coexistence model.

Table 5: Comparison of coexistence and Gneuss-Greiner model predictions of reduced E2 transition rates in ^{44}Ca.

Table 6. Composition of states in ^{44}Ca [18].

TABLE 1

	^{40}Ca	^{42}Ca	^{44}Ca	^{46}Ca
P_2	33.33	14.29	20.97	3.97
P_3	10.76	-11.35	78.33	-0.07
C_2	1020.2	110.2	-48.78	518.25
C_3	1.78	0.0	349.0	148.3
C_4	-10524	-622.5	1134.2	-24241
C_5	9.17	189.3	26.12	26629
C_6	1409.5	0.0	-1471.8	-56568
D_6	30277	1275.7	498.9	481130

TABLE 2

TRANSITION FROM	TO	THEORY [1]	THEORY [22]	EXP [3]	GG
$2_1^+(K=0,4p4h)$	$0_1^+(K=0,0p0h)$	6	10	18±2	13
	$0_2^+(K=0,4p4h)$	253	340	250±35	26
$2_2^+(K=2,4p4h)$	$0_1^+(K=0,0p0h)$	0	0.1	0.8±0.1	0
	$0_2^+(K=0,4p4h)$	7.5	3.8	6.5±3.3	9
	$2_1^+(K=0,4p4h)$	124	135	140±40	386
$4_1^+(K=0,4p4h)$	$2_1^+(K=0,4p4h)$	370	480	535±110	402
$3_1^+(K=2,4p4h)$	$2_1^+(K=0,4p4h)$	10	6.5	32±8	11
	$2_2^+(K=2,4p4h)$	440	626	730±300	417
	$4_1^+(K=0,4p4h)$	-	-	<180	166
$4_2^+(K=2,4p4h)$	$2_1^+(K=0,4p4h)$	3.9	15	35^{+20}_{-11}	9
	$2_2^+(K=2,4p4h)$	115	188	200^{+150}_{-75}	223
	$4_1^+(K=0,4p4h)$	64	78	52±44	192

TABLE 3

TRANSITION FROM	TRANSITION TO	THEORY(q_{eff}=0.75)	THEORY(q_{eff}=1.0)	EXP	GG
2_1^+	0_1^+	66	102	83±3	84
0_2^+	2_1^+	565	777	556±34	855
2_2^+	0_1^+	4	4	15±2	3
	2_1^+	95	134	88^{+92}_{-59}	223
	0_2^+	157	223	<594	334
4_1^+	2_1^+	114	171	65±7	*347
	2_2^+	20	25	484^{+245}_{-195}	425
6_1^+	4_1^+	19	31	6.4±0.1	*945
4_2^+	2_1^+	157	217	136±41	14
	2_2^+	203	294	542±300	262
2_3^+	0_1^+	3	3	3.4±1.0	3
	2_1^+	48	66	65±20	51
	0_2^+	10	12	17.5±5.3	58
	2_2^+	39	52	~20	133

TABLE 4

STATE	$^{42}Ca^{\dagger}$ (%) $\lvert(f_{7/2})^2\rangle$	$\lvert$deformed$\rangle$	^{40}Ca (%) $\lvert$0p0h$\rangle$	$\lvert$2p2h$\rangle$ K=0	2	4	$\lvert$4p4h$\rangle$ 0	2	4
0_1^+	77	13	82	17			1		
2_1^+	38	51	0	10	~0		88	2	
0_2^+	12	87	3	2			94		
2_2^+	47	48	0	~0	7	~0	2	91	
4_1^+	66	27	0	6	1	~0	76	17	~0
6_1^+	94	4	0	2	1	~0	63	33	1
4_2^+	27	72	0	2	4	~0	16	78	~0

† the balance is made up of fp, ff, p and f spherical configurations.

TABLE 5

TRANSITION FROM	TRANSITION TO	THEORY	EXP	GG
2_1^+	0_1^+	85	85±15	92
0_2^+	2_1^+	265	200±60	292
4_1^+	2_1^+	120	160±60	210
2_2^+	2_1^+	60	>60	10
2_2^+	0_1^+	1	>24	3
4_2^+	4_1^+	2	15^{+60}_{-10}	6
4_2^+	2_1^+	2	2.5±0.6	6
6_1^+	4_1^+	70	50±12	*314

TABLE 6

STATE	$\%(f_{7/2})^4$ (ν=0,2)	$\%(f_{7/2})^4$ (ν=4)	$\%\|$rotational deformed$\rangle$
0_1^+	74	-	26
0_2^+	26	-	74
2_1^+	45	2	53
2_2^+	54	7	39
2_3^+	~1	~92	~8
4_1^+	31	26	43
4_2^+	34	64	2
6_1^+	80	-	20

FIGURE CAPTIONS:

Figure 1: Potential energy surfaces of $^{40,42,44,46}Ca$ in the a_0 and a_2 plane. Lines of equipotential are in MeV. Also shown are cuts taken along the γ-directions where the (deformed) minima

Figure 2: Low energy spectrum and quadrupole moments of ^{40}Ca calculated in the Gneuss-Greiner (GG) and compared with experiment (EXP)

Figure 3: Comparison of calculated (GG) and experimental (EXP) low energy spectra and quadrupole moments of $^{42,44}Ca$.

Figure 4: Low lying properties of ^{46}Ca as predicted by the Gneuss-Greiner model (GG) and compared with the available experimental data

Figure 5: Photoneutron and photoproton cross section data [23] for ^{40}Ca compared with the Gneuss-Greiner model prediction (full curve).

Figure 6: Total absorption cross section of ^{42}Ca [24] compared with the predictions of the Gneuss-Greiner model. Also shown are the main dipole strengths ψ (= $\langle 1_n \| D \| 0 \rangle$).

Figure 7: Total absorption cross section of ^{44}Ca [25] compared with the predictions of the Gneuss-Greiner model. Also shown are the main dipole strengths ψ (= $\langle 1_n \| D \| 0 \rangle$).

Figure 8: Total absorption cross section of ^{46}Ca as predicted by the Gneuss-Greiner model. Vertical lines indicate the main dipole strengths ψ (= $\langle 1_n \| D \| 0 \rangle$).

Figure 9 Predicted elastic (0_1^+) and inelastic (2_1^+) scattering cross sections at θ=135° for the calcium isotopes The cross sections for scattering to the 0_2^+, 2_2^+ and 2_3^+ states are negligible (<2μb/sr).

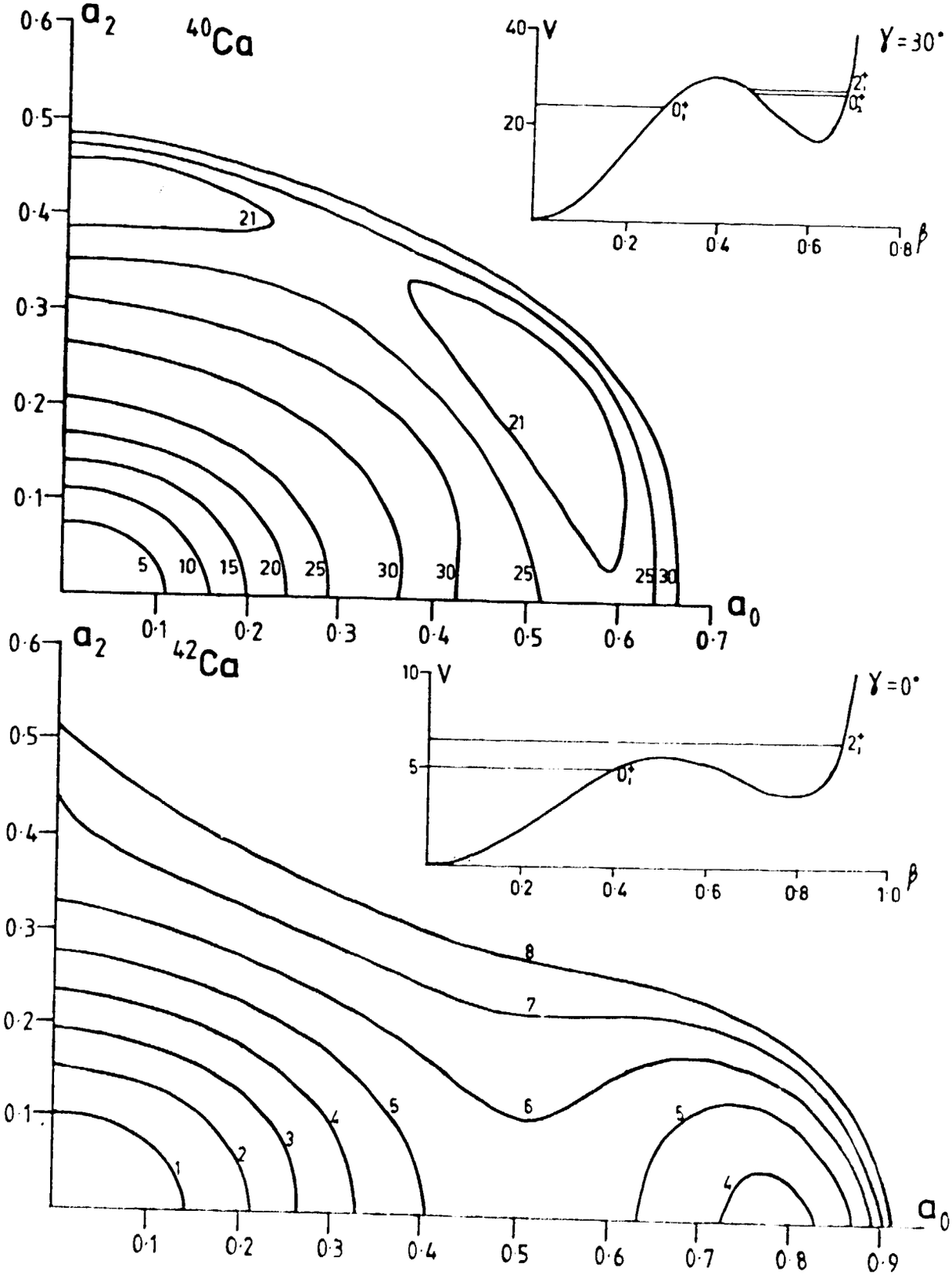
a_2
^{40}Ca
0·6
0·5
0·4
0·3
0·2
0·1
21
21
5
10
15
20
25
30
30
25
25
30
0·1
0·2
0·3
0·4
0·5
0·6
0·7
a_0
40
V
20
0_1^+
2_1^+
0_2^+
$\gamma = 30°$
0·2
0·4
0·6
0·8
β
a_2
^{42}Ca
0·6
0·5
0·4
0·3
0·2
0·1
8
7
6
5
4
3
2
1
5
4
0·1
0·2
0·3
0·4
0·5
0·6
0·7
0·8
0·9
a_0
10
V
5
0_1^+
2_1^+
$\gamma = 0°$
0·2
0·4
0·6
0·8
1·0
β

Figure 1

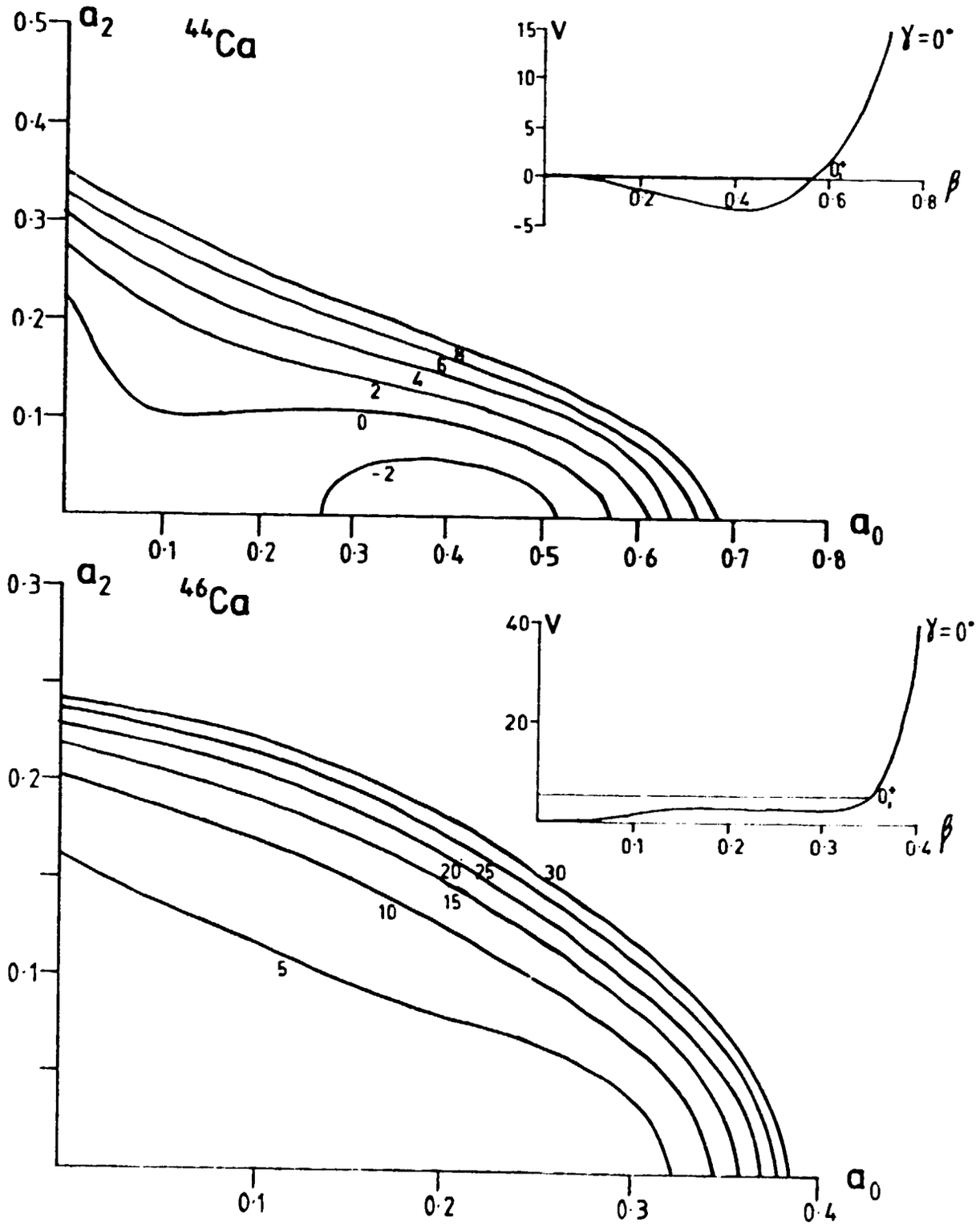

Figure 1 (cont.)

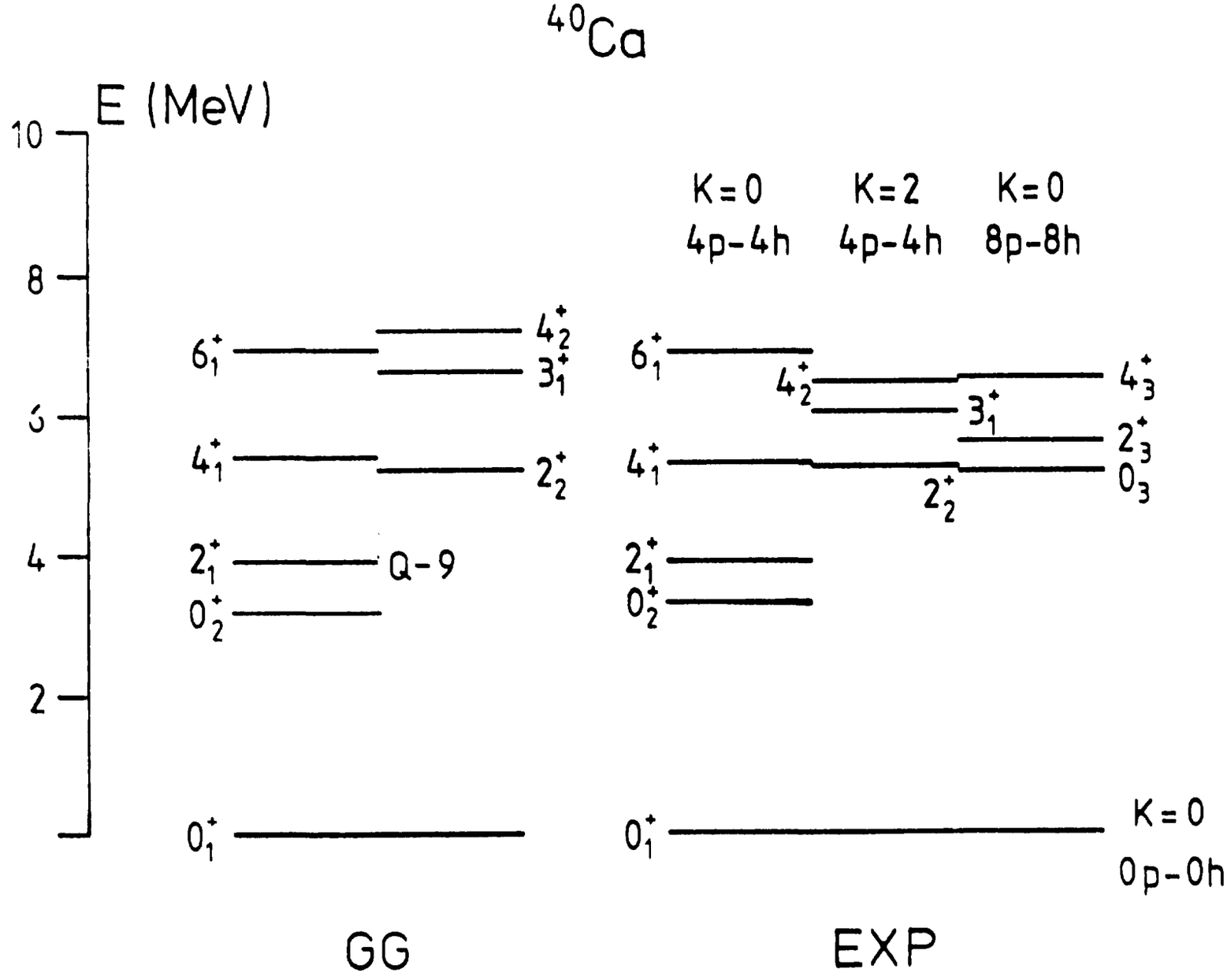
^{40}Ca
E (MeV)
10
8
6
4
2
K=0
4p-4h
K=2
4p-4h
K=0
8p-8h
6_1^+
4_2^+
3_1^+
4_1^+
2_2^+
2_1^+
0_2^+
0_1^+
Q-9
4_3^+
2_3^+
0_3^+
K=0
0p-0h
GG
EXP

Figure 2

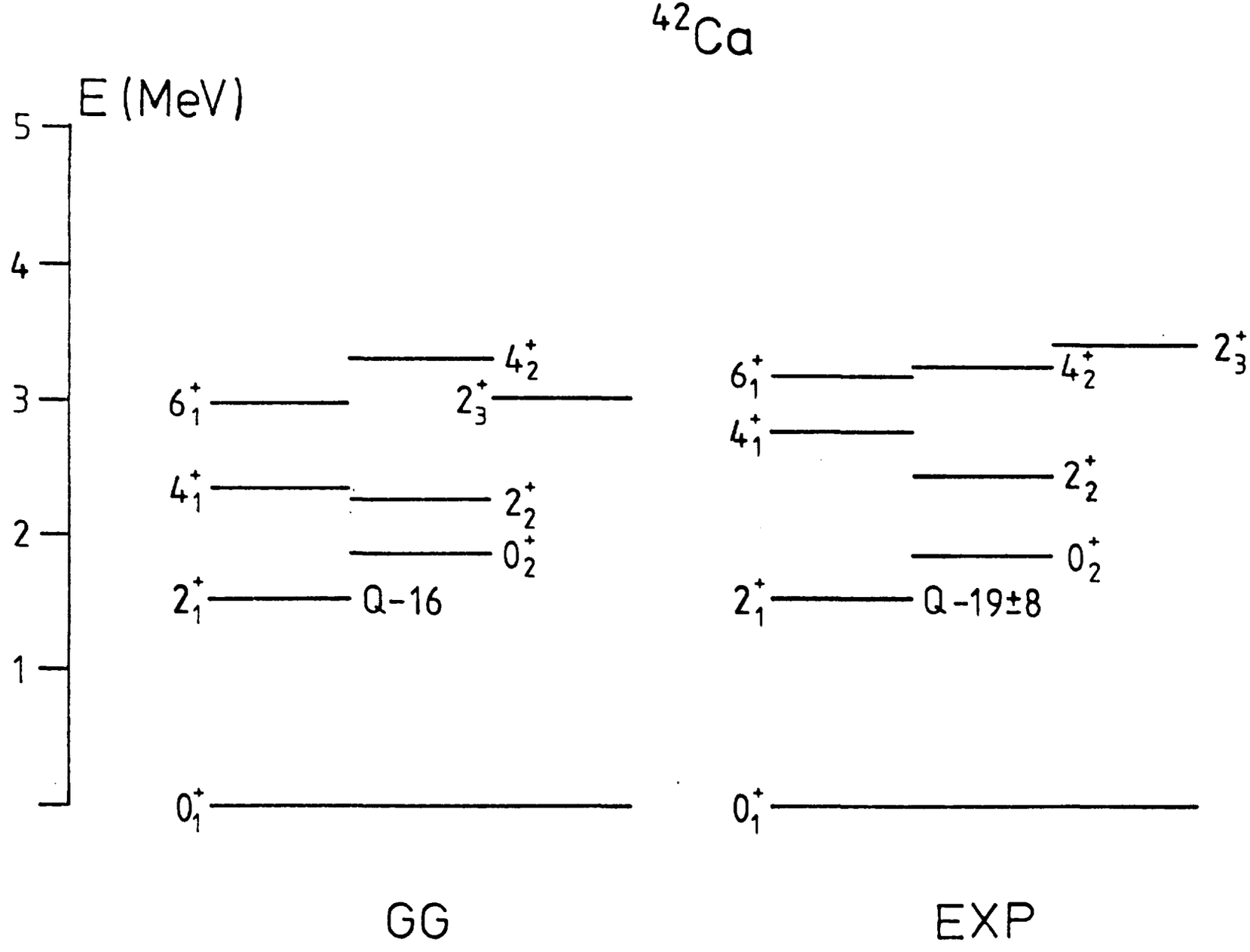
^{42}Ca
E (MeV)
5
4
3
2
1
6_1^+
4_2^+
2_3^+
4_1^+
2_2^+
0_2^+
2_1^+
Q-16
0_1^+
GG
6_1^+
4_2^+
2_3^+
4_1^+
2_2^+
0_2^+
2_1^+
Q-19±8
0_1^+
EXP

Figure 3

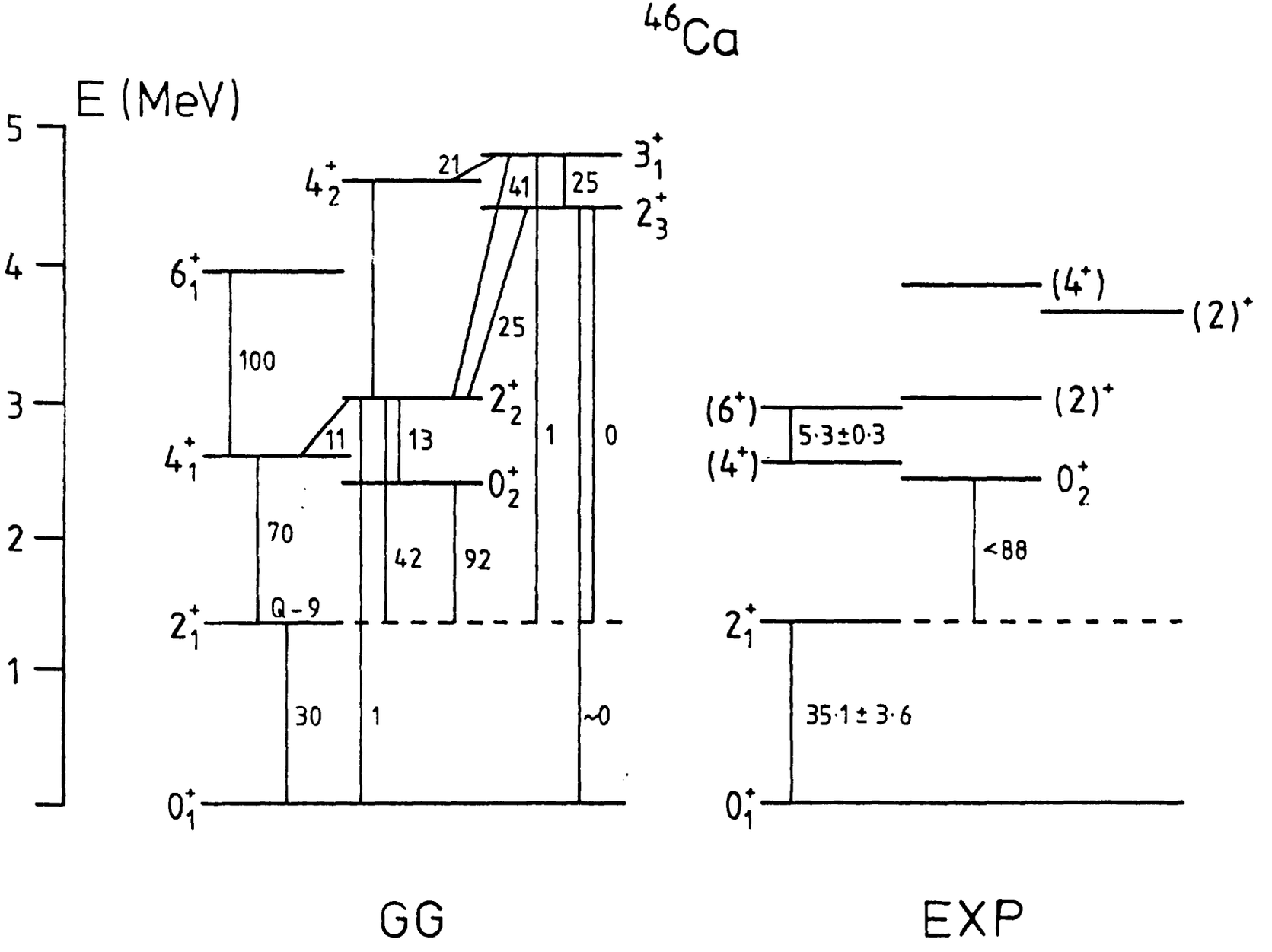
^{46}Ca
E (MeV)
5
4
3
2
1
4_2^+
3_1^+
2_3^+
6_1^+
2_2^+
4_1^+
0_2^+
2_1^+
0_1^+
21
41
25
25
100
11
13
1
0
70
42
92
Q-9
30
1
~0
GG
(4⁺)
(2)⁺
(6⁺)
(2)⁺
5·3±0·3
(4⁺)
0_2^+
<88
2_1^+
35·1 ± 3·6
0_1^+
EXP

Figure 4

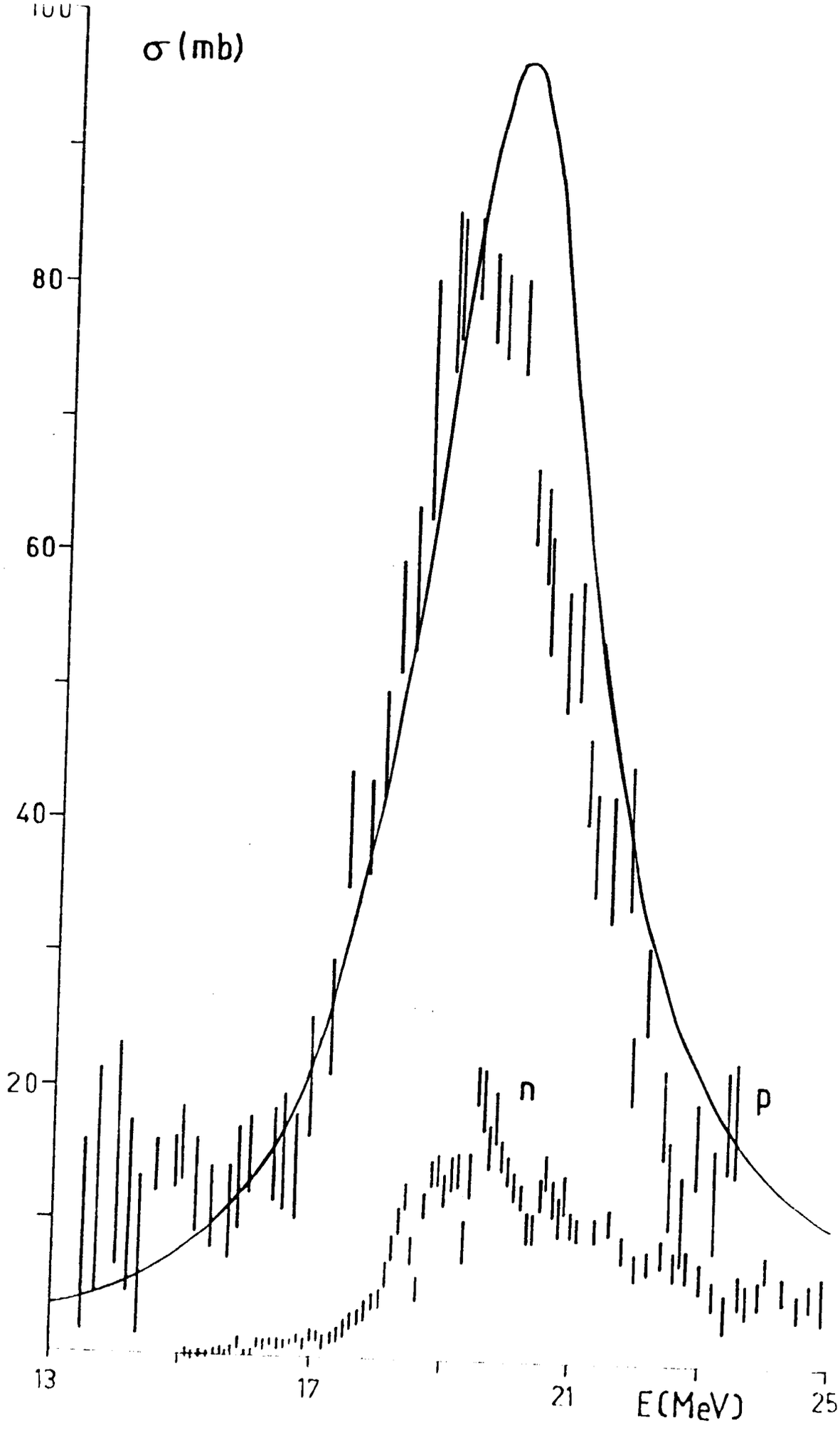

Figure 5

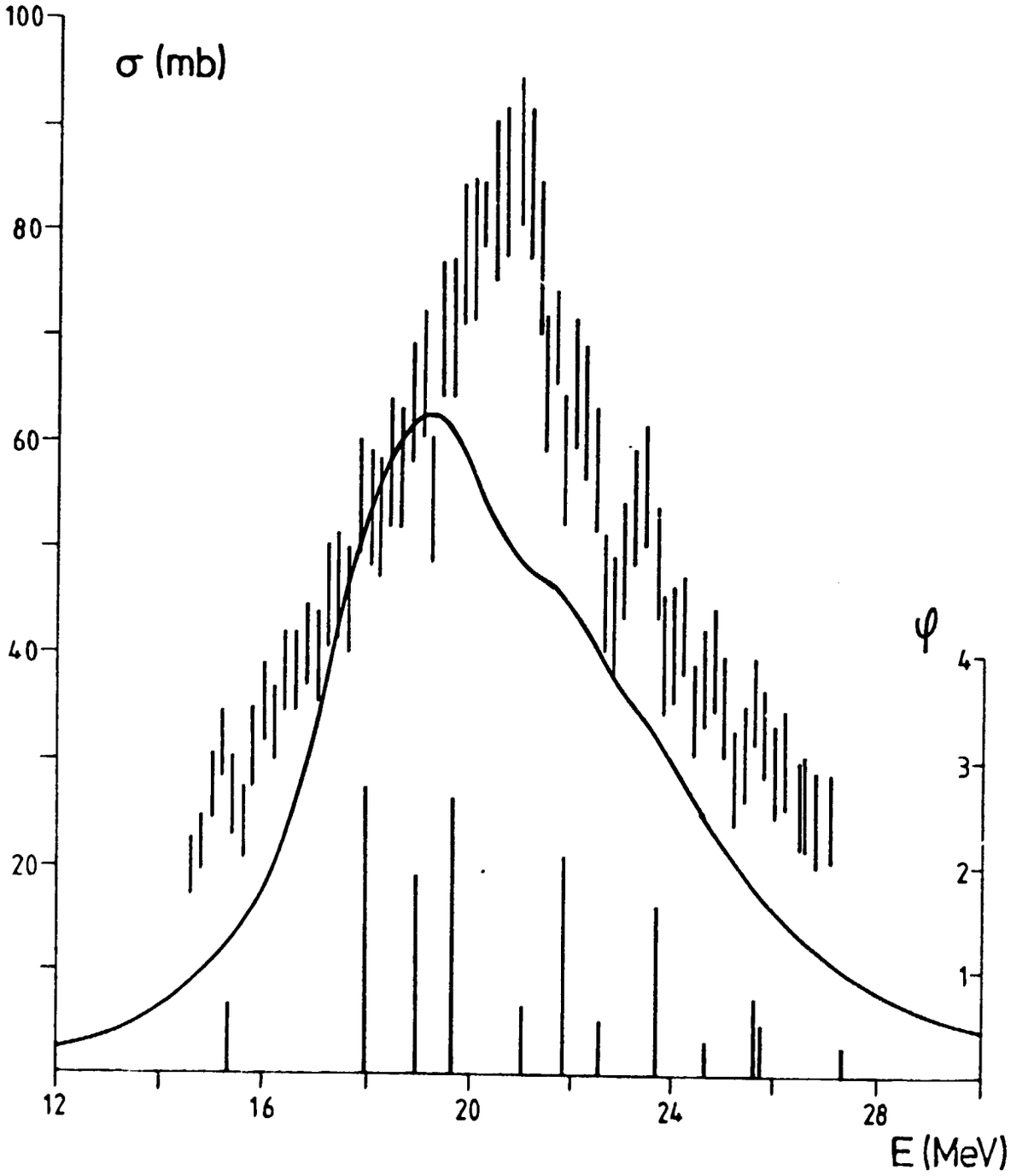

Figure 6

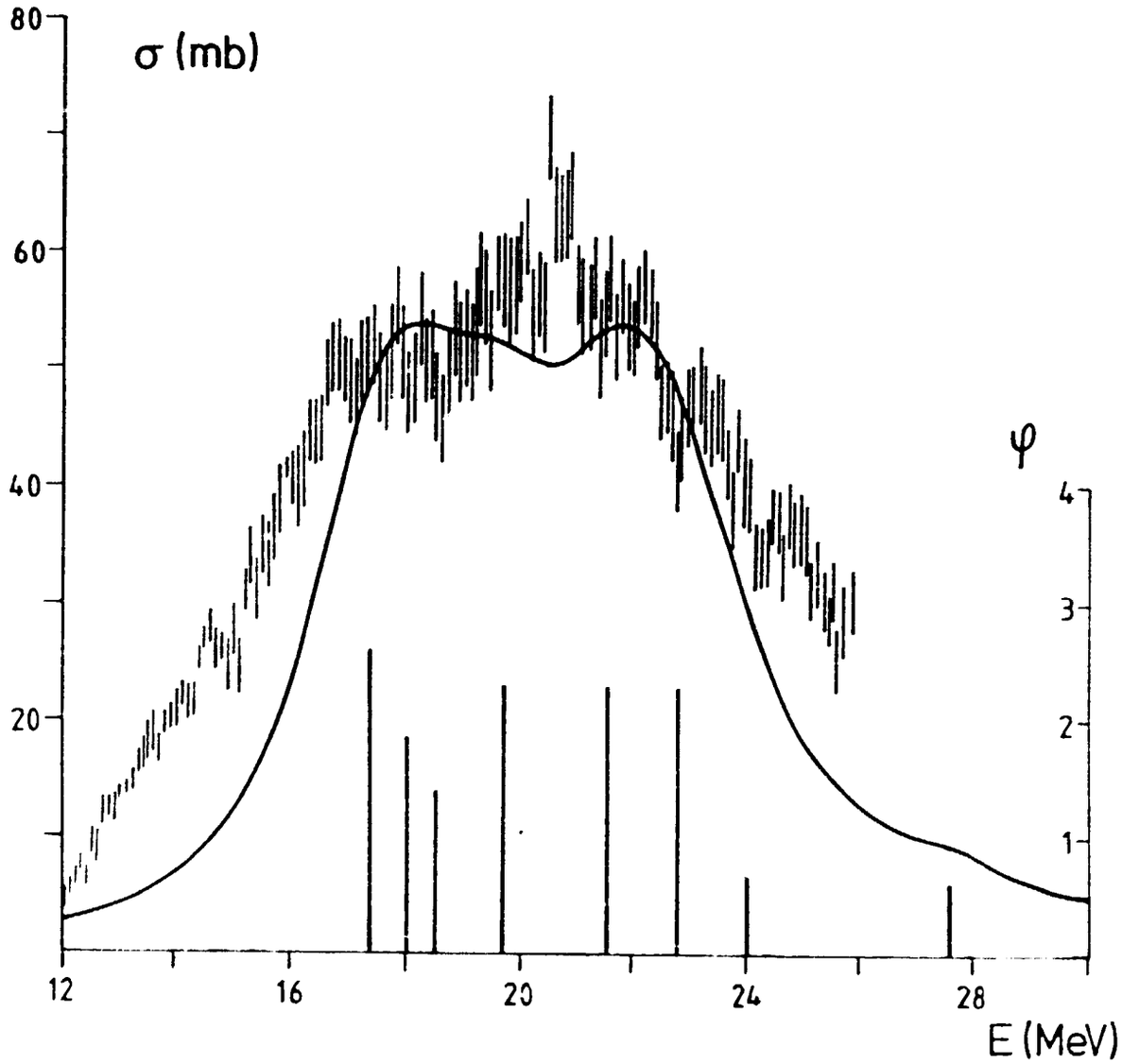

Figure 7

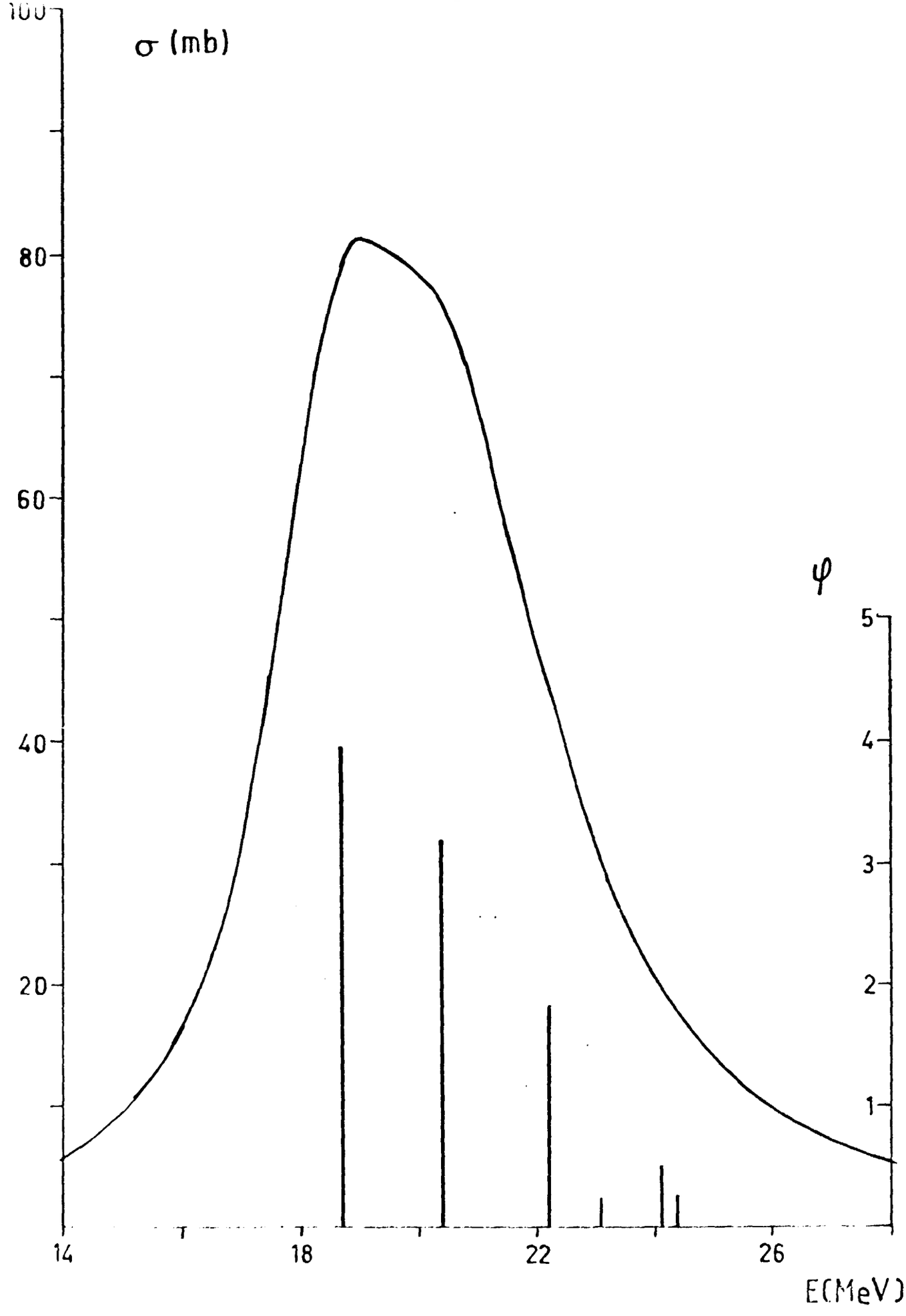

Figure 8

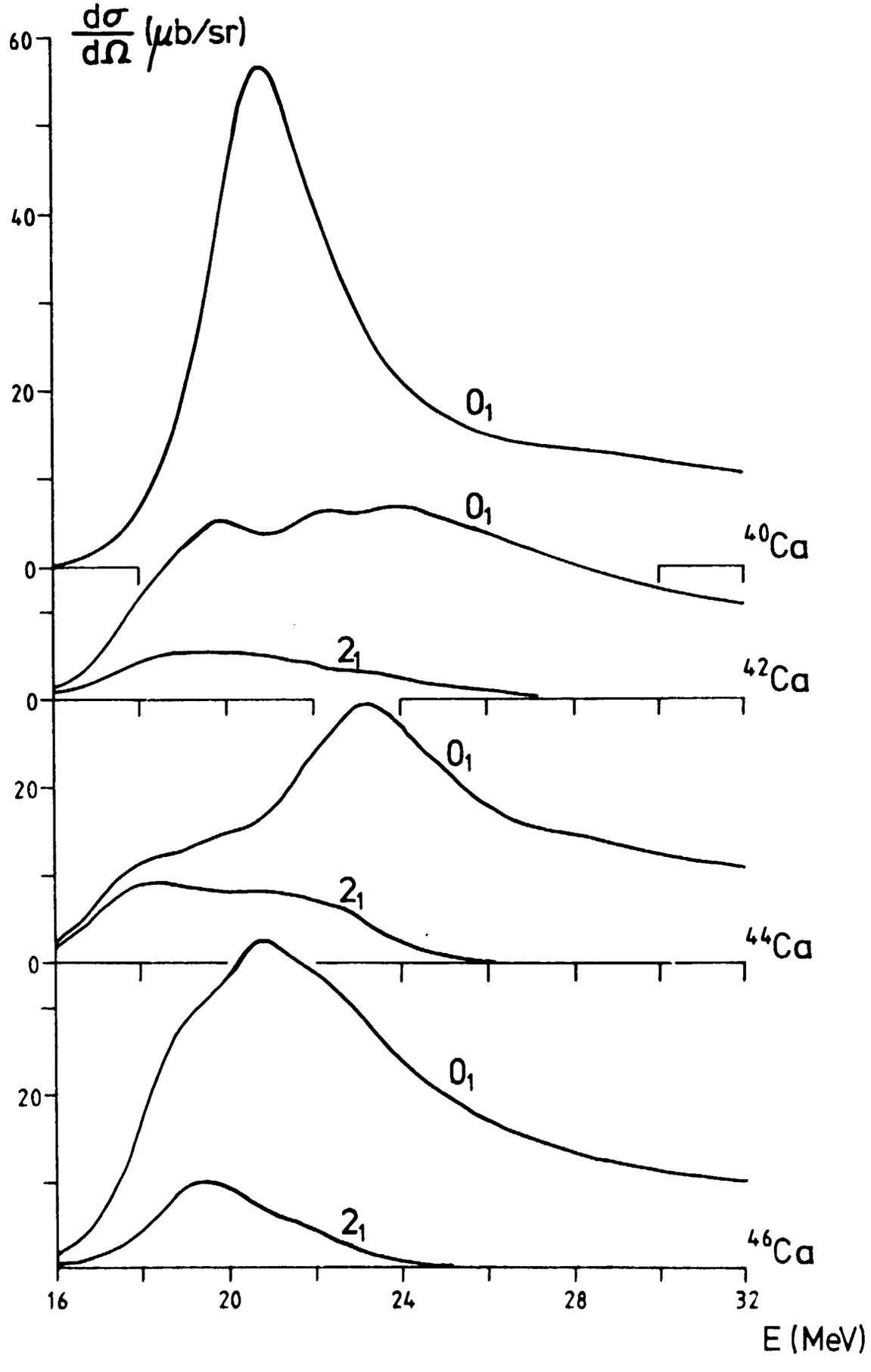
dσ/dΩ (μb/sr)
60
40
20
0
0₁
0₁
40Ca
2₁
42Ca
0
20
0₁
2₁
44Ca
0
20
0₁
2₁
46Ca
16
20
24
28
32
E (MeV)

Figure 9